HHS Public Access

Author manuscript

Nat Chem. Author manuscript; available in PMC 2023 July 01.

Published in final edited form as:

Nat Chem. 2023 January ; 15(1): 101–109. doi:10.1038/s41557-022-01057-1.

Targeted activation in localized protein environments via deep red photoredox catalysis

Nicholas Eng Soon Tay[1,‡], **Keun Ah Ryu**[2,‡], **John L. Weber**[1], **Aleksandra K. Olow**[3], **David C. Cabanero**[1], **David R. Reichman**[1], **Rob C. Oslund**[2,4,*], **Olugbeminiyi O. Fadeyi**[2,4,*], **Tomislav Rovis**[1,*]

[1]Department of Chemistry, Columbia University, 3000 Broadway, New York, NY, 10027, USA

[2]Exploratory Science Center, Merck & Co., Inc., Cambridge, MA, 02139, USA

[3]Genetics and Pharmacogenomics, Merck & Co., Inc., South San Francisco, CA, 94080, USA

[4]Current Address: InduPro, Cambridge, MA, 02142, USA

Abstract

State-of-the art photoactivation strategies in chemical biology provide spatiotemporal control and visualization of biological processes. However, using high energy light ($\lambda < 500$ nm) for substrate or photocatalyst sensitization can lead to background activation of photoactive small molecule probes and reduce its efficacy in complex biological environments. Here we describe the development of targeted aryl azide activation via deep red light ($\lambda = 660$ nm) photoredox catalysis and its use in photocatalyzed proximity labeling. We demonstrate that aryl azides are converted to triplet nitrenes via a redox-centric mechanism and show that its spatially localized-formation requires both red light and a photocatalyst-targeting modality. This technology was applied in different colon cancer cell systems for targeted protein environment labeling of epithelial cell adhesion molecule (EpCAM). We identified a small subset of proteins with previously known and unknown association to EpCAM, including CDH3, a clinically relevant protein that shares high tumor selective expression with EpCAM.

Graphical Abstract

[*]Corresponding authors: rob@induprolabs.com, niyi@induprolabs.com, tr2504@columbia.edu.
[‡]These authors contributed equally

Author contributions

N.E.S.T., K.A.R., R.C.O., O.O.F., and T.R. conceived of the work. N.E.S.T., K.A.R., A.K.O., D.C.C., R.C.O., O.O.F., and T.R. designed and executed experiments. N.E.S.T., K.A.R., D.C.C., R.C.O., O.O.F., and T.R. interpreted results. J.L.W and D.R.R. designed and executed chemistry-based computations. J.L.W. and D.R.R. interpreted chemistry-based computational results. N.E.S.T., K.A.R., R.C.O., O.O.F., and T.R. wrote the manuscript with input from all authors.

Competing Interests Statement

K.A.R., A.K.O., R.C.O., and O.O.F. were employed by Merck Sharp & Dohme Corp., a subsidiary of Merck & Co., Inc., Kenilworth, NJ, USA., during the experimental planning, execution and/or preparation of this manuscript. The remaining authors declare no competing interests.

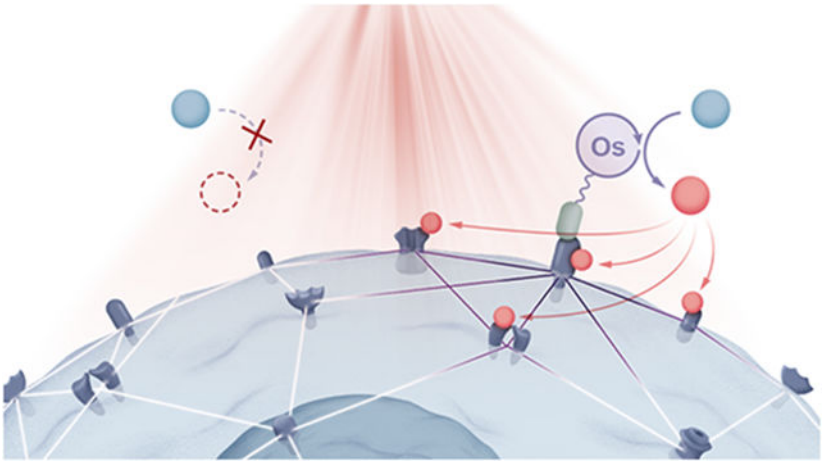

Editorial Summary:

Technologies for profiling biological environments with high spatiotemporal resolution are in-demand to enable the discovery of new targets for addressing unmet clinical needs. Now, a deep red light mediated photocatalytic strategy for the targeted activation of aryl azides has been developed. This platform enables mapping of protein microenvironments in physiologically relevant systems.

New targeted activation strategies are essential for uncovering fundamental biological processes that inspire clinical applications. From methods that enable cellular microenvironment mapping to technologies that hijack biological machinery, fulfilling this translational promise requires a deep understanding of the chemical principles that underlie these tools. A prime example is the use of aryl azides which has widespread use in many chemical biology-based applications within the context of photoaffinity labeling (PAL)[1,2], photo-uncaging[3,4], protein conjugation[5,6,7,8], protein cross-linking[9], and enzyme-mediated protein labeling[10]. Of these approaches, the ability to activate aryl azides via ultraviolet (UV) or visible light irradiation has surfaced as a highly attractive approach for labeling, uncaging, or conjugation (Fig. 1A). However, limitations such as unselective/background labeling, a requirement for high energy light, and the generation of multiple reaction pathways from current photoactivation methods restrict downstream biological applications. As a consequence, direct photolysis presents challenges for activation of aryl azides in a spatially-controlled manner. This has important implications for profiling protein interactions within complex physiological environments. Thus, low-energy light driven technologies that enable spatio-temporal activation of aryl azides are highly desirable.

The identity of the aryl azide plays an important role in determining the photoactivation reaction pathways (Fig. 1B). For example, singlet aryl nitrene (**1**) ($t_{1/2}$~ 1–10 ns)[11] is formed via UV photolysis of unsubstituted aryl azides. This leads to rapid two-step rearrangement to the benzazirine and subsequent ring-expansion to a long-lived 7-membered ketenimine (**2**) that is susceptible to hydrolysis or nucleophilic trapping ($t_{1/2}$~ 5 ms–1 s depending on the concentration of intercepting species)[12,13,14]. To overcome this limitation, perfluorinated aryl azides (PFAA) have been adopted[15,16] to enable complementary reactivity through

the singlet nitrene, leading to *N*-centered covalent adducts[17,18]. This intermediate can additionally relax via intersystem crossing (ISC) ($k_{ISC} \sim 10^6$–10^7 s^{-1})[19] to a triplet nitrene[20,21], which has divergent reactivity relative to its singlet form[17,21,22]. Given that multiple reactive pathways are generated through direct high energy light photoactivation, identifying methods that incorporate lower energy light systems and do not directly activate aryl azides (Fig. 1B), would allow for a targeted activation platform in physiologically relevant environments.

Visible-light photocatalysis is an emerging strategy for probing complex biological systems as the selective delivery of photons enables catalytic, chromoselective substrate activation via the controlled formation of high-energy species that covalently bind to desired biomolecule targets.[23] To fully realize the potential of visible light, a paradigm shift in photoactivation must turn focus from substrate to catalyst, and low energy wavelengths of light—ideally in the deep red (DR) or near-infrared (NIR) range ($\lambda > 600$ nm)— used to maximize the physiological relevance of photocatalytic applications. To achieve this goal, the discovery and implementation of new systems involving localized, catalytic activation of latent chemical probes will be key. In particular, recent endeavors of photoredox catalysis via light-induced electron transfer (ET) or energy transfer (EnT) into chemical biology have been particularly fruitful, leading to early-stage applications for cancer phototherapy[24] and proximity labeling[25]. In the latter example, carbene intermediates are used, as they offer a tight labeling radius ($t_{1/2} \sim 4$ ns), but suffer from background quenching with water and oxygen in their singlet and triplet forms, respectively.[26] Replacing these reactive species with triplet nitrenes, which are less sensitive to reactions with oxygen[17,27] and protic solvents[18], will improve reactivity with biomolecules in complex physiological environments relative to carbenes. Additionally, versatility of aryl azides beyond proximity labeling, especially within the context of targeted photo-uncaging via azide-to-aniline reduction, should encourage exploratory efforts into new mechanisms for aryl azide activation and localized drug delivery.[4]

Although photocatalytic approaches utilizing high-energy blue light (450 nm) to form the nitrene intermediate via ET[28] or EnT[29,30] mechanisms have been reported, the potential for direct photoactivation of aryl azides through these methods hinder their utility for probing biological environments in a targeted fashion. In view of this limitation, we sought to develop a new low energy light-based catalytic platform for biomolecule labeling via triplet nitrene generation (Fig. 1C). Recently, we disclosed a method for DR and NIR photoredox catalysis where osmium photocatalysts harvest low-energy light to facilitate synthetic reactions via ET and EnT[31]. We therefore envisioned a DR light-based photocatalytic labeling approach in which an osmium complex is tethered to a targeting modality for localized generation of reactive triplet nitrene species within the desired region of a complex biological system (Fig. 1D). Given the inherent value of understanding protein communities within disease states such a technology would unlock new strategies for selective therapeutic development. With this in mind, here we report the development of a DR light-mediated photoredox technology and use it to profile the local protein environment of EpCAM, a tumor selective antigen, within different colon cancer monoculture, spheroid, and dissociated tumor tissue cell systems.

Results and discussion

Overcoming aryl azide photolytic limitations with deep red photoredox catalysis.

To examine the impact of blue light irradiation on background azide activation (Fig. 2A), we performed a trapping experiment with nonfluorinated azide **3**, which is known to form a ketenimine intermediate upon photolysis. Using 468 nm LEDs, we observed 85% yield of azepine **4** alongside a 5% yield of aniline **5**. This result was surprising as it suggests that irradiating the absorption region tail of azide **3** is sufficient to induce azide photolysis (Fig. 2B). To probe the activation mechanism, we irradiated azide **3** in the presence of catalytic iridium photocatalyst (**6**) — a well-documented triplet sensitizer with an excited state oxidation potential ($E(Ir^{IV/III*})$ = −0.89 V vs SCE) insufficient for ET-mediated azide activation. Contrary to expected azepine product, we instead isolated aniline **5** in 75% yield, with only 3% of **4** observed. This result suggests that aryl azide activation via energy transfer results in a triplet nitrene formation that does not produce the ketenimine immediate as previously proposed.[30] Noting that one-electron reduction pathways can lead to aniline formation, we used an osmium photocatalyst (**7**) with a greater redox match ($E(Os^{III/II*})$ = −1.05 V vs SCE) with the azide reduction potential ($E_{p/2}$ = −1.25 V vs SCE), and obtained **5** in 85% yield when irradiated with 468 nm LEDs. Given the broadband absorption of photocatalyst **7** and its defined triplet metal-ligand charge transfer (^{3}MLCT) band in the 530–700 nm range (Fig. 2B), we were interested in the effects of decoupling azide light- and redox-dependent activation pathways. When the azide is irradiated with 660 nm LEDs in the absence of photocatalyst, full recovery of the azide is observed whereas when **7** is added, 50% conversion of **3** to **5** is observed. These results reveal that (1) no background activation is observed under red light irradiation, (2) light and redox decoupling is unviable when using blue light, (3) an exergonic redox match between the photocatalyst and azide may be necessary for efficient activation. To investigate this latter point, we examined the conversion of perfluorinated azide **8** ($E_{p/2}$ = −0.79 V vs. SCE) to aniline **9**, and found that quantitative formation of **9** was observed in an hour, with 2-hydroxytetrahydrofuran as the only byproduct (Fig. 2C). The reaction is dependent on the reducing ability of the photocatalyst rather than triplet energy as photocatalysts **10** and **11**, which have similar triplet energies but lower $E(Os^{III/II*})$, are less efficient at converting the azide to aniline.

Importantly, we further found this aniline reduction method displays broad substrate compatibility within the context of PFAA featuring several commonly-used bio-orthogonal probes (Fig. 2D). Simple functional groups such as benzamide (**12**), benzyl alcohol (**13**), nitrile (**14**), biotin (**15**), sugar (**16**–**19**), and tryptamine (**20**) substrates are unaffected, with the aniline obtained in near quantitative yields. Bioorthogonal groups such as alkyl azide (**21**) and alkyne (**22**) are also unreactive, with the former example notable as the conditions developed by Liu and coworkers activate both alkyl and aryl azides[28]. Alkyl diazirine (**23**) is also compatible with the reduction, highlighting the potential for achieving tandem photoactivation using diazirine and PFAA as complementary photoactivatable groups. Finally, we found that this photocatalytic reduction strategy may be used for prodrug release, as shown by catalytic reduction and uncaging of PFAA-bound hydroxycoumarin, sugars, and doxorubicin (Supplementary Fig. 1). It is important to note that the uncaging of the aniline

is dependent on azide electronics[32] and modulating this property should enable its use in catalytic prodrug activation.

Computational modeling of aryl azide activation via deep red photoredox catalysis

We next undertook density functional theory (DFT) calculations to elucidate the potential mechanism for obtaining triplet nitrene. We ruled out Dexter EnT as a viable pathway as the vertical and adiabatic singlet-to-triplet energies (ΔG = 88.3 and 63.3 kcal/mol respectively) necessary for obtaining the triplet azide **25** are significantly greater than the triplet energy of the osmium photocatalyst **7** (ΔG = 44.8 kcal/mol).[33] By contrast, we found an ET transfer mechanism to be energetically favorable as the reduced azide (**26**) could be significantly stabilized through both solvation and fluorination (Fig. 3A). Additionally, we found that the barrier to N_2 dissociation upon reduction is minimal (Fig. 3B) and, as expected, N_2 loss is highly exothermic (Fig. 3A). Subsequent exothermic re-oxidation of the reduced nitrene (**27**) by $\mathbf{7}^+$ then reveals the triplet nitrene (**28**). Thus, we propose a photoredox-catalyzed, stepwise reduction-dissociation-oxidation pathway occurs (Fig. 3C), taking advantage of the stability of charged intermediates to form triplet nitrene **28**. This novel mechanism is further supported by qualitative trends with solvation and fluorination; using a solvent with a lower dielectric constant or replacing fluorine with hydrogen raises the energy of the anionic azide (whereas the triplet energy remains approximately identical), resulting in a lower reaction completion rate (Supplemental Fig. 2, and Supplemental Table 1).

Divergence in nitrene reactivity between azide photolysis and redox-mediated azide activation.

To further confirm the triplet nitrene pathway, we compared the product distributions for our method against UV- or blue-light photolysis for toluene (Fig. 4, top) and dimethyl sulfoxide (Fig. 4, bottom). UV photolysis of **8** in the presence of toluene yields a mixture of aryl and benzylic amination products (**29** and **30** respectively), whereas our DR photoredox method yields only the benzylic C–H insertion product from toluene, as well as azobenzene **31**. Observing the latter product is important as it is indicative of triplet nitrene formation[11,21]. Blue-light photolysis of **8** in dimethylsulfoxide leads to quantitative formation of sulfoximine **32** whereas our DR photoredox method yields a 1:1 mixture of **31** and **32**. Furthermore, investigation of additional reaction partners reveals general reactivity with $C(sp^3)$–H bonds, alkenes, and sulfides with azide **8** under DR photoredox conditions (Supplemental Fig. 3), suggesting the utility of exploiting triplet perfluoroaryl nitrenes to label within biological environments where many of these functional groups can be found. Taken together, these results show that our photoredox method enables high-energy nitrene formation with low-energy light via a redox mechanism, and the resulting triplet perfluorinated aryl nitrenes have similar reactivity to their singlet counterparts, although stepwise mechanisms are likely involved.

Deep red photoredox-catalyzed azide activation for protein labeling

Having identified DR photoredox conditions that induce activation of various PFAAs, we next investigated the application of this method to achieve covalent protein labeling in aqueous buffer conditions. In anticipation of utilizing this photocatalyst system in a targeted

fashion within biological environments, we designed an osmium photocatalyst containing an alkyne linker for easy attachment to targeting modalities (Supplemental Fig. 4). As a proof-of-concept experiment, we combined carbonic anhydrase (CA) with PFAA-biotin (**15**) and free osmium-alkyne photocatalyst followed by irradiation with red light (660 nm) using a recently developed biophotoreactor[34] (Fig. 5A). Under these conditions, we observed biotinylation of CA in the presence of both the photocatalyst and red light whereas the absence of light or the use of red light without photocatalyst does not induce biotinylation (Fig. 5B). Comparable results were achieved using osmium photocatalysts without the alkyne linker (Supplemental Fig. 5). Also, similar to our chemical transformation results in Fig. 2, we found that the direct exposure of PFAA to blue light led to biotinylation with CA (Fig. 5B), further highlighting that background labeling can occur from direct activation of aryl azides with higher energy wavelengths of light. Finally, we investigated protein labeling as a function of red-light exposure time and observed increasing biotinylation levels as a function of light duration confirming the light dependent nature of our labeling system (Fig. 5C).

Targeted EpCAM microenvironment mapping in colorectal cancer cell systems

Light dependent protein labeling via our DR photoredox technology opens the possibility to achieve targeted labeling of protein environments within cell-based systems. Accordingly, we selected EpCAM to test the concept of targeted protein labeling on the surface of live cancer cells. EpCAM is highly expressed on the cancer cell surface and can be easily targeted with available antibody tools for localized delivery of the osmium-alkyne photocatalyst. We therefore targeted EpCAM in three different HCT116 cell systems with our osmium photocatalyst followed by irradiation with DR light to induce cell surface biotinylation for downstream protein enrichment, mass spectrometry-based proteomics, and bioinformatic analysis (Fig. 6A). Targeted labeling of EpCAM was performed using a two-antibody system that consists of a primary α-EpCAM antibody and secondary antibody labeled with an osmium-alkyne photocatalyst (Supplemental Fig. 4) that binds to the primary antibody. HCT116 cells were labeled with the primary and secondary antibodies followed by addition of PFAA-biotin and DR-light irradiation. Similar to our protein labeling experiments, western blot analysis showed increased protein biotinylation that correlates with irradiation time (Fig. 6B). As a negative control, targeted labeling with a non-binding isotype control primary antibody and secondary antibody photocatalyst resulted in background levels of protein biotinylation (Fig. 6B). To investigate the potential of our DR photoredox system to generate reactive oxygen species (ROS) that can damage cellular environments, we measured singlet oxygen and hydrogen peroxide generation and observed minimal to no ROS increase compared to no light controls (Supplemental Figs. 6 and 7). This result was also consistent with the observation that cell viability is not affected by DR-light irradiation of cells labeled with the osmium-conjugated antibody system (Supplemental Fig. 8). Collectively, these results highlight compatibility of our osmium photocatalyst system for profiling within live cell environments.

With this photocatalytic targeting system in hand, we investigated EpCAM protein microenvironments on HCT116 cells within three distinct cell systems. This includes HCT116 cells grown in monoculture and detached in single cell suspension, grown in

3-D spheroid culture, or dissociated cells from mice tumor xenograft tissue (Fig. 6A). In each of these cell systems, EpCAM targeted biotinylation was performed with our primary/secondary antibody system followed by cell lysis and streptavidin bead-based enrichment of labeled proteins. Streptavidin-enriched proteins were then identified and quantified using TMT-based LC-MS/MS proteomic analysis. Volcano plot analysis was then performed to identify statistically significant enriched proteins that resulted from EpCAM targeting. In each of the cell systems, EpCAM was detected as highly enriched confirming the ability of our technology to label and enrich the targeted protein (Supplemental Figs. 9-11). As a comparison to other proximity labeling methods that target and enrich EpCAM from the cell surface, we performed similar labeling experiments using either a peroxidase enzyme that generates a phenoxy radical for protein labeling or an iridium photocatalyst[25] for carbene-based proximal protein labeling. Using a secondary antibody conjugated to horseradish peroxidase (HRP) or to the iridium photocatalyst, we performed targeted labeling via the primary anti-EpCAM antibody on HCT116 cells grown in monoculture. While proximity labeling via HRP in the presence of biotin phenol resulted in enrichment of EpCAM and other proteins in similar fashion to our osmium/PFAA method, the overall number of significantly enriched proteins was nearly 10-fold higher with HRP (Supplemental Fig. 12). In contrast, using the iridium photocatalyst in the presence of diazirine biotin led to dramatic enrichment of EpCAM over other proteins and, unlike the osmium/PFAA system, fewer proteins were enriched with the iridium/diazirine method (Supplemental Fig. 12). This observation is consistent with the shorter labeling radius of the carbene intermediate that has shorter half-life than the nitrene generated by osmium/PFAA. These collective results highlight the suitability of osmium/PFAA for broadly surveying proximal protein regions over state-of-the-art methods.

The high expression of EpCAM on many different tumor types has led to intense focus of EpCAM as a tumor associated antigen and biomarker[35,36]. Thus, enhancing our understanding of EpCAM cancer cell surface microenvironments can provide additional avenues for development of tumor-selective therapeutics and biomarker-based diagnostics. We therefore focused our attention on other commonly enriched membrane proteins, in addition to EpCAM, identified by our DR photocatalytic labeling technology. The surface proteins CD109, CD44, CDCP1, CDH3, DCBLD2, DDR1, DSC2, DSG2, ITGA2, ITGA3, NT5E, PTGFRN were enriched in at least two of the tested cell systems with EpCAM, CD44, CDH3, ITGA2, ITGA3 being enriched in all three (Fig. 6C). Of note, a recent study utilizing BioID-mediated extracellular and intracellular proximity labeling of E-cadherin collectively identified over 1000 proteins wherein EPCAM and CDH3 were both co-enriched within the extracellular and cytosolic E-cadherin protein environments[37].

The search tool for retrieval of interacting genes (STRING)[38] was used to obtain protein–protein interaction (PPI) network information for these proteins revealing both known and inferred protein interactions (Fig. 6D). Further bioinformatic analysis of GO terms associated with proteins enriched in two or more cell systems resulted in the identification of biological processes associated with EpCAM function that include cellular adhesion, junction organization, and migration (Supplemental Fig. 13). Interestingly, comparing the EpCAM proximal proteins identified with our method (Fig. 6C) to a recently published EpCAM immunoprecipitation study[39] or to protein interaction databases (Bioplex[40],

Biogrid[41]) revealed mostly new interactions (19/21), highlighting the intrinsic differences between our technology that achieves direct covalent labeling on live cell surfaces and immunoprecipitation methods used in other studies (Supplemental Fig. 14).

We next explored the gene expression profile for these enriched proteins across tumor vs normal tissue using data obtained from The Cancer Genome Atlas (TCGA) and Genotype-Tissue Expression (GTEx), respectively. In addition to EpCAM, several genes (CDH3, DSG2, CDCP1, DSC2, and ITGA2) showed increased gene expression levels in tumor over normal tissue (Fig. 6E). Given our HCT116 cell system is derived from colorectal cancer, we performed a breakdown of gene expression for each of the enriched proteins by tumor indication (Fig. 6F) and observed increased tumor-associated gene expression across different tumor types including increased gene expression in colorectal tumors for EpCAM, CDH3, and DSG2. We further analyzed gene co-expression analysis of EpCAM and each of the other enriched genes across individual primary tumor colon adenocarcinoma samples from TCGA and healthy colon and large intestine samples from GTEX and observed high co-expression with EpCAM in most of the identified hits, with the exception of NUP155, CD109 and DCBLD2 (Fig. 6G). Of note, co-expression of EpCAM with CDH3 appears to be highly specific to primary colon adenocarcinoma tumors over normal tissue, highlighting the potential utility of co-targeting these two genes for increased tumor specificity in colon adenocarcinomas.

Conclusion

In summary, we developed a photoredox strategy to generate high-energy nitrenes via low-energy light that proceeds through a redox-neutral electron transfer process. The resulting azide activation yields only triplet nitrene and operates solely when osmium photocatalyst and red light are used. These prerequisites enable the use of our photocatalytic system for targeted labeling applications wherein a photocatalyst can be directed to a cellular region of interest for localized activation of aryl azide probes. This strategy has particularly important implications for profiling biological environments with high spatiotemporal resolution. compared to other proximity labeling methods. For example, enzyme-based BioID generates a long-lived biotin-AMP intermediate ($t_{1/2}$ ~ 1 min), whereas peroxidase-generated phenoxy radical ($t_{1/2}$ ~ 100 μs)[42] that has a comparable half-life to the triplet nitrene ($t_{1/2}$ ~ 200 μs)[43] produced by our technology. Whereas most enzyme-based approaches rely on fusion to the target of interest, our system requires a targeting modality that is delivered to the protein of interest. Thus, this photocatalyst-based approach enables the proximity profiling of endogenous protein environments without additional genetic engineering requirements. Furthermore, in comparison to other photocatalytic proximity labeling methods, the use of tissue-penetrating DR light for photocatalyst activation to generate a nitrene intermediate can potentially overcome both the limitations of blue light penetrance and the restrictive labeling radius of highly reactive carbene species for profiling proximal environments, particularly in more physiologically complex tissue systems.

We applied this osmium-based photocatalytic system for the targeted labeling of EpCAM on the surface of live colorectal cancer cells to identify not only EpCAM, but a small subset of neighboring surface proteins. The success of this technology opens up possibilities

for probing other membrane proteins of interest with the intent of developing cell surface-focused therapeutics and diagnostics. While the two-antibody system we currently use affords high modularity with a wide range of protein targets and efforts towards developing smaller photocatalyst-protein constructs (e.g. single-antibody, expressed protein, etc.) to shorten the labeling radius are currently ongoing. Furthermore, we anticipate that this mode of triplet nitrene activation will uncover new chemical reactivity and invite new applications for synthesis and chemical biology. Accordingly, efforts to further develop photocatalytic-based bioorthogonal activation modes that make use of low-energy light in tissue environments are underway.

Methods

Synthesis of osmium photocatalyst 33

Dichlorobis(3,4,7,8-tetramethyl-1,10-phenanthroline)osmum(II)—The title compound was prepared according to a published procedure, spectral data are in agreement with literature values.[1]

[Bis(1,10-phenanthroline)-dppz]osmium(II) hexafluorophosphate—To a clean, dry pressure vessel equipped with a stir bar (heavy wall, 10 mL), was added dichlorobis(3,4,7,8-tetramethyl-1,10-phenanthroline)osmum(II) (93.2 mg, 0.15 mmol, 1 equiv) and dppz (48.0 mg, 0.17 mmol, 1.1 equiv). The vessel was then moved into a nitrogen glovebox, where 4 mL of ethylene glycol was added. The reaction was then sealed and heated on a sand bath at 200 °C for 1 hour (reaction will turn from a brown-dark pink suspension to a black-brown solution). Upon reaction completion, the vessel is cooled to room temperature and diluted with excess ammonium hexafluorophosphate (> 20 equiv) and DI water (~5-10 mL). The suspension is stirred for 10 minutes before filtration over a Buchner funnel equipped with filter paper (Fisherbrand P4, medium porosity). The black-brown precipitate is washed with DI water and diethyl ether. (**Note**: precipitate is readily soluble in polar organic solvents). The precipitate is dried under reduced pressure and purified using column chromatography on basic alumina gel (50% DCM:MeCN to 100% MeCN) to give the title product in 80% yield (134.7 mg). **Note**: The product contains small amounts of tris(3,4,7,8-tetramethyl-1,10-phenanthroline)osmium (II) hexafluorophosphate, for which the signals have been identified. This side product can be separated with additional chromatography.

[Bis(3,4,7,8-tetramethyl-1,10-phenanthroline)-(5-(4-CONH-PEG4-alkyne)-Ph)-Phen]osmium(II) hexafluorophosphate (33)—To a clean, dry 20 dram vial equipped with a stir bar was added osmium precursor [bis(1,10-phenanthroline)-dppz]osmium(II) hexafluorophosphate (94.0 mg, 0.075 mmol, 1 equiv), HATU (57.0 mg, 0.15 mmol, 2 equiv) and DMF (0.1 M). Then, alkyne-PEG-4 amine (26.0 mg, 0.11 mmol, 1.5 equiv, dissolved in ~0.5-1 mL DMF) was added to the reaction via syringe before DIPEA (0.13 mL , 0.75 mmol, 10 equiv) was added. The reaction was allowed to stir for 24 h under N_2 with TLC (5 % MeOH:DCM on basic alumina) monitoring of reaction progress. When the reaction is complete, the reaction is concentrated under reduced pressure before purification by column chromatography on basic alumina. The loaded column

is first eluted with 1:1 DCM:MeCN to 100% MeCN to remove tris(3,4,7,8-tetramethyl-1,10-phenanthroline)osmium (II) hexafluorophosphate before changing the mobile phase to 1% MeOH:DCM to 10% MeOH:DCM to obtain the title product as a black-brown solid in 25% yield (27.5 mg). If further purification is required, the isolated compound can be repurified using column chromatography on silica gel (1% MeOH:DCM to 10% MeOH:DCM).

General experimental conditions for photoredox-catalyzed azide-to-aniline reduction.—To a clean, dry 1 dram vial containing a Teflon-coated magnetic stir bar was added the specified azide substrate (0.10 mmol, 1 equiv). The vial was moved into a N_2 glovebox where 1:1 THF:DI H_2O (1.0 mL, 0.1 M, H_2O is argon sparged) and 10 mM solution of photocatalyst **7** in MeCN (50 μL, 0.0005 mmol, 0.5 mol%) were added in sequential order. The vial was then sealed with a Teflon-lined septum screw cap, removed from the glovebox, positioned on a stir plate approximately 5 cm from a Kessil PR160-660 LED Photoredox Light supplying deep red light (λ = 660 nm) and irradiated for 12 h. The crude reaction mixture was then diluted with CD_3CN (1 mL) and fluorobenzene standard (0.10 mmol), and analyzed by ^1H NMR and ^{19}F NMR. The crude product is then concentrated under reduced pressure and purified using column chromatography on silica gel (conditions specified for each example).

Experimental Procedures for Biological Applications

General cell culture protocol—HCT116 cells were cultured in Roswell Park Memorial Institute (RPMI) 1640 1X medium containing L-Glutamine (Corning, 10-040-CV), 10% fetal bovine serum (FBS) (HyClone, SH30910.03) and 100 IU Penicillin/100μg/mL Streptomycin (1X from a 100X stock, Corning, 30-002-CI). After preparation, all cell culture media was sterilized using 0.2 μm Nalgene™ Rapid-Flow™ Sterile Disposable Filter Units with PES Membrane, 1,000 mL capacity (Thermo Scientific, 567-0020) or 500 mL capacity (Thermo Scientific, 569-0020) as needed and stored at 4 °C until ready to use. All cells were grown at 37 °C with 5% CO_2 in 25cm^2 (Corning: 430639), 75cm^2 (Corning: 430641U) or 150 cm^2 (Corning: 430825) canted neck, vented cap sterile cell culture. For passaging of adherent cells, cells were detached from the plate using Trypsin-EDTA (0.05%, Gibco, 25300054) as indicated.

General Protein Labeling—Photocatalyst (5 μM) was combined with PFAA-biotin (250 μM, Thermo fisher 21303) and protein of interest (1 mg/mL) in DPBS to afford reaction mixtures. The reaction mixtures were irradiated with 660 nm light in a biophotoreactor for 15 minutes at 100% intensity. 30 μL samples were then removed, combined with 10 μL of 4x reducing Laemmli sample buffer (5% 2-mercaptoethanol), vortexed, and heated at 95 °C for 10 minutes. 10 μL of each sample was then analyzed by Western blot according to the Western Blot General Protocol.

Western blot—Gel electrophoresis was performed using a Bio-Rad Criterion Vertical Electrophoresis Cell tank, Bio-Rad PowerPac Basic Power Supply, and Criterion TGX tris-glycine polyacrylamide gel cassettes (SDS/Tris). After electrophoresis, gels were transferred from precast cassettes to PVDF membranes using an iBlot 2 gel transfer device (Thermo Fisher, IB21001, IB23001). The membranes were immersed in Blocking Buffer (3% BSA

in TBST) and incubated at r.t. for 1 hour. The blocking solution was then decanted, and 35 mL of fresh blocking buffer containing 30 μL of IRDye 800CW streptavidin (Li-Cor, 926-32230) was added and the mixture incubated at 4 °C overnight. The membranes were washed with 1X TBST (3 x 5 min) and water before imaging via Li-Cor Odyssey CLx scanner in the 800 nm channel. Pixel densitometry was performed using Image Studio Lite V. 5.2 (Li-Cor). The streptavidin 800 channel pixel density was then divided by the total protein stain 700 channel pixel density to provide a normalized biotinylation signal for each protein band.

Total protein staining—Following gel electrophoresis, the gel was washed in water, and immersed in simply blue safestain (Thermo fisher LC6060) and left to incubate at r.t. for 1 hour. The membrane was rinsed with water x2 and left to destain in 20% NaCl (w/v) in DI water overnight. Gel was subsequently imaged via Li-Cor Odyssey CLx scanner in the 800 nm channel. Pixel densitometry was performed using Image Studio Lite V. 5.2 (Li-Cor).

Monoculture cell viability in presence of osmium conjugated antibodies—Viability of cells during the proximity labeling procedure was measured by following the proximity labeling procedures. As a further control, 5 μM of photocatalyst and 250 μM of PFAA-biotin were added to 1 million cells in 1 mL PBS, and incubated at r.t. on a rotator for the duration of the proximity labeling procedure. After irradiation, cells were collected and analyzed by MTT assay following manufacturer's protocol (Thermofisher M6494).

Antibody-mediated Targeted Labeling Protocol

Antibody conjugation—The following operations were carried out at room temperature. 150 μL of a 2.0 mg/mL stock of goat α-mouse polyclonal antibody (Millipore, AP124) was combined with 15 μL of 1.0 M NaHCO3 and 10 μL of a 10 mM stock of NHS-PEG4-azide (Thermo fisher 26130) in DMSO. The mixture was incubated for 1.5 hours. After this time, the reaction mixture was passed through a ZEBA 40 kDa 2 mL desalting column which had been equilibrated with Tris-HCl (pH 8.0, 50 mM). The Tris-HCl solution (ca. 200 μL) was then treated with Osmium-alkyne (**33**) in DMSO (final concentration 200μM), then the components of the Click-It kit (Thermo Fisher Scientific, C10276) were added: 15 μL $Cu(OAc)_2$, and 15 μL additive 1. The mixture was incubated for 5 minutes, then 30 μL additive 2 was added and the mixture allowed to incubate in the dark for 30 minutes. The reaction mixture was then passed through a DPBS-equilibrated desalting column to afford ca. 250 μL of Osmium-antibody stock. The photocatalyst-antibody conjugate was analyzed by BCA protein assay kit (Thermo Fisher) for total protein concentration and absorbance at 350 nm for Os catalyst concentration against serial dilutions of respective standards. The typical conjugation ratio was 1:6 (antibody:photocatalyst) using these conditions.

Dissociated tumor tissue labeling protocol—Samples were purchased from Charles River Laboratories as frozen dissociated tumor tissue cells derived from an HCT116 CDX model. Cells were pelleted, the supernatant removed, and then resuspended in 1 mL of cold DPBS containing 20 μg Isotype control (BD Biosciences, Purified Mouse IgG1 κ, clone MOPC-21, 556648) or 20 μg purified mouse α-human EPCAM antibody (Invitrogen, clone 323/A3, MA5-12436). The cells were incubated on a rotisserie for 30 min at room

temperature. After incubation, the cells were pelleted to remove the supernatant and washed twice with 1 mL cold DPBS. After the final wash, the cells were pelleted to remove the supernatant and resuspended in 1 mL of cold DPBS containing 20 μg of photocatalyst-conjugated goat α-mouse secondary IgG and incubated on a rotisserie for 30 min at room temperature. After incubation, the cells were pelleted to remove the supernatant, washed twice with 1 mL cold DPBS and resuspended in 1 mL of cold DPBS containing 250 μM PFAA-biotin. The samples were then irradiated in a biophotoreactor for 15 min (100% intensity) at 660 nm. After irradiation, the cells were then pelleted to remove the supernatant and washed with DPBS and pelleted. Cell pellets were further processed for western blot analysis (general western blot procedure), or proteomics sample preparation (general proteomics preparation procedure).

Monoculture labeling protocol—20 million HCT116 cells were used for each reaction condition. Cell suspensions were transferred to Protein LoBind tubes in 1 mL aliquots. The cells were pelleted, the supernatant removed, and then resuspended in 1 mL of cold DPBS containing 20 μg Isotype control (BD Biosciences, Purified Mouse IgG1 κ, clone MOPC-21, 556648) or 20 μg purified mouse α-human EPCAM antibody (Invitrogen, clone 323/A3, MA5-12436). The cells were incubated on a rotisserie for 30 min at room temperature. After incubation, the cells were pelleted to remove the supernatant and washed twice with 1 mL cold DPBS. After the final wash, the cells were pelleted to remove the supernatant and resuspended in 1 mL of cold DPBS containing 20 μg of photocatalyst-conjugated goat α-mouse secondary IgG and incubated on a rotisserie for 30 min at room temperature. After incubation, the cells were pelleted to remove the supernatant, washed twice with 1 mL cold DPBS and resuspended in 1 mL of cold DPBS containing 250 μM PFAA-biotin. The samples were then irradiated in a biophotoreactor for 15 min (100% intensity) at 660 nm. After irradiation, the cells were then pelleted to remove the supernatant and washed with DPBS and pelleted. Cell pellets were further processed for western blot analysis (general western blot procedure), or proteomics sample preparation (general proteomics preparation procedure).

HCT116 spheroids culture protocol—HCT116 cells were plated in 96 well ultra-low attachment microplates (Corning, 07-201-680) at 20,000 cells/ well. The cells were grown for 5 days, resulting in approximately double the number of cells (4-5 million cells/ plate/ reaction condition). Spheroids in each full plate were collected in Protein LoBind tubes by pipetting out each spheroid with a 1000 μL pipette with a cut off tip to maintain the morphology of the spheroid. The spheroids were washed briefly in PBS twice, and resuspended in 500 μL of PBS containing 5 μg Isotype control (BD Biosciences, Purified Mouse IgG1κ, clone MOPC-21, 556648) or 5 μg purified mouse α-human EPCAM antibody (Invitrogen, clone 323/A3, MA5-12436). The cells were incubated at 37C for one hour. Following incubation, the supernatant was removed and the spheroids were rinsed with PBS x2. Following the quick rinse, the cells were incubated in 1 mL PBS at 37C for 5 min three times. After the final wash, the cells were resuspended in 500 μL of PBS containing 5 μg of photocatalyst-conjugated goat α-mouse secondary IgG and incubated 37C for one hour. Following the rinse and wash procedures, the cells were resuspended in 1 mL of DPBS containing 250 μM PFAA-biotin and incubated at 37C for 5 mins before irradiation for

15 minutes (100% intensity) at 660 nm in the biophotoreactor. After irradiation, the cells were then pelleted to remove the supernatant and washed with DPBS and pelleted. Cell pellets were further processed for western blot analysis (general western blot procedure), or proteomics sample preparation (general proteomics preparation procedure).

Supplementary Material

Refer to Web version on PubMed Central for supplementary material.

Acknowledgements

Research was supported by the NIH National Institute of General Medical Sciences (R01- GM125206) and gifts from Merck & Co., Inc., Kenilworth, New Jersey, USA. J.L.W was funded in part by the Columbia Center for Computational Electrochemistry (CCCE). This work used the Extreme Science and Engineering Discovery Environment (XSEDE), which is supported by National Science Foundation grant number ACI-1548562[44]. In particular, we used San Diego Computing Center's Expanse resources under allocation ID COL151.

Data Availability Statement

Data supporting the main findings of this study are available in the Article, Supporting Information and Source Data. All supplementary figures, experimental details and synthesis information are included in the Supplementary Information. Unprocessed proteomics results are available in the Supplementary Data Table. Raw proteomics data are deposited on MassIVE (public data access: ftp://massive.ucsd.edu/MSV000088973/).

References

1. Kotzyba-Hibert F, Kapfer I & Goeldner M Recent Trends in Photoaffinity Labeling. Angew. Chem. Int. Ed 34, 1296–1312 (1995).
2. Murale DP, Hong SC, Haque Md. M. & Lee J-S Photo-affinity labeling (PAL) in chemical proteomics: a handy tool to investigate protein-protein interactions (PPIs). Proteome Science 15, 14 (2017). [PubMed: 28652856]
3. Sadhu KK, Eierhoff T, Römer W & Winssinger N Photoreductive Uncaging of Fluorophore in Response to Protein Oligomers by Templated Reaction in Vitro and in Cellulo. J. Am. Chem. Soc 134, 20013–20016 (2012). [PubMed: 23186060]
4. Geng J et al. Switching on prodrugs using radiotherapy. Nat. Chem 13, 805–810 (2021). [PubMed: 34112990]
5. Holland JP, Gut M, Klingler S, Fay R & Guillou A Photochemical Reactions in the Synthesis of Protein–Drug Conjugates. Chem. Eur. J 26, 33–48 (2020). [PubMed: 31599057]
6. Fantoni NZ, El-Sagheer AH & Brown T A Hitchhiker's Guide to Click-Chemistry with Nucleic Acids. Chem. Rev 121, 7122–7154 (2021). [PubMed: 33443411]
7. Deb T, Tu J & Franzini RM Mechanisms and Substituent Effects of Metal-Free Bioorthogonal Reactions. Chem. Rev 121, 6850–6914 (2021). [PubMed: 33400520]
8. Heiss TK, Dorn RS & Prescher JA Bioorthogonal Reactions of Triarylphosphines and Related Analogues. Chem. Rev 121, 6802–6849 (2021). [PubMed: 34101453]
9. Chin JW et al. Addition of *p*-Azido-L-phenylalanine to the Genetic Code of Escherichia coli. J. Am. Chem. Soc 124, 9026–9027 (2002). [PubMed: 12148987]
10. Kotani N et al. Biochemical visualization of cell surface molecular clustering in living cells. Proc. Natl. Acad. Sci. U.S.A 105, 7405–7409 (2008). [PubMed: 18495923]
11. Gritsan NP & Platz MS Kinetics, Spectroscopy, and Computational Chemistry of Arylnitrenes. Chem. Rev 106, 3844–3867 (2006). [PubMed: 16967923]

12. DeGraff BA, Gillespie DW & Sundberg RJ Phenyl nitrene. Flash photolytic investigation of the reaction with secondary amines. J. Am. Chem. Soc 96, 7491–7496 (1974).
13. Li YZ, Kirby JP, George MW, Poliakoff M & Schuster GB 1,2-Didehydroazepines from the photolysis of substituted aryl azides: analysis of their chemical and physical properties by time-resolved spectroscopic methods. J. Am. Chem. Soc 110, 8092–8098 (1988).
14. Marcinek A & Platz MS Deduction of the activation parameters for ring expansion and intersystem crossing in fluorinated singlet phenylnitrenes. J. Phys. Chem 97, 12674–12677 (1993).
15. Liu L-H & Yan M Perfluorophenyl Azides: New Applications in Surface Functionalization and Nanomaterial Synthesis. Acc. Chem. Res 43, 1434–1443 (2010). [PubMed: 20690606]
16. Xie S, Sundhoro M, Houk KN & Yan M Electrophilic Azides for Materials Synthesis and Chemical Biology. Acc. Chem. Res 53, 937–948 (2020). [PubMed: 32207916]
17. Poe R, Schnapp K, Young MJT, Grayzar J & Platz MS Chemistry and kinetics of singlet pentafluorophenylnitrene. J. Am. Chem. Soc 114, 5054–5067 (1992).
18. Soundararajan N & Platz MS Descriptive photochemistry of polyfluorinated azide derivatives of methyl benzoate. J. Org. Chem 55, 2034–2044 (1990).
19. Marcinek A et al. Unusually long lifetimes of the singlet nitrenes derived from 4-azido-2,3,5,6-tetrafluorobenzamides. J. Phys. Chem 98, 412–419 (1994).
20. Schnapp KA, Poe R, Leyva E, Soundararajan N & Platz MS Exploratory photochemistry of fluorinated aryl azides. Implications for the design of photoaffinity labeling reagents. Bioconjugate Chem. 4, 172–177 (1993).
21. Keana JFW & Cai SX New reagents for photoaffinity labeling: synthesis and photolysis of functionalized perfluorophenyl azides. J. Org. Chem 55, 3640–3647 (1990).
22. Kanakarajan K, Goodrich R, Young MJT, Soundararajan S & Platz MS EPR spectroscopy of triplet aryl nitrenes covalently bound to α-chymotrypsin. Application of low-temperature methods to photoaffinity labeling. J. Am. Chem. Soc 110, 6536–6541 (1988).
23. Ryu KA, Kaszuba CM, Bissonnette NB, Oslund RC & Fadeyi OO Interrogating biological systems using visible-light-powered catalysis. Nat Rev Chem 5, 322–337 (2021).
24. Huang H et al. Targeted photoredox catalysis in cancer cells. Nat. Chem 11, 1041–1048 (2019). [PubMed: 31548671]
25. Geri JB et al. Science. 367, 1091–1097 (2020). [PubMed: 32139536]
26. Wright MH & Sieber SA Chemical Proteomics Approaches for Identifying the Cellular Targets of Natural Products. Nat. Prod. Rep 33, 681–708 (2016). [PubMed: 27098809]
27. Liu J, Hadad CM & Platz MS The Reaction of Triplet Nitrenes with Oxygen: A Computational Study. Org. Lett 7, 549–552 (2005). [PubMed: 15704891]
28. Chen Y, Kamlet AS, Steinman JB & Liu DR A biomolecule-compatible visible-light-induced azide reduction from a DNA-encoded reaction-discovery system. Nat. Chem 3, 146–153 (2011). [PubMed: 21258388]
29. Farney EP & Yoon TP Visible-Light Sensitization of Vinyl Azides by Transition-Metal Photocatalysis. Angew. Chem. Intl. Ed 53, 793–797 (2014).
30. Wang H et al. Selective Mitochondrial Protein Labeling Enabled by Biocompatible Photocatalytic Reactions inside Live Cells. JACS Au 1, 1066–1075 (2021). [PubMed: 34467350]
31. Ravetz BD et al. Development of a Platform for Near-Infrared Photoredox Catalysis. ACS Cent. Sci 6, 2053–2059 (2020). [PubMed: 33274281]
32. Matikonda SS et al. Mechanistic Evaluation of Bioorthogonal Decaging with trans-Cyclooctene: The Effect of Fluorine Substituents on Aryl Azide Reactivity and Decaging from the 1,2,3-Triazoline. Bioconjugate Chem. 29, 324–334 (2018).
33. Ásgeirsson V et al. Nudged Elastic Band Method for Molecular Reactions Using Energy-Weighted Springs Combined with Eigenvector Following. J. Chem. Theory Comput 17, 4929–4945 (2021). [PubMed: 34275279]
34. Bissonnette NB et al. Design of a Multiuse Photoreactor To Enable Visible-Light Photocatalytic Chemical Transformations and Labeling in Live Cells. ChemBioChem 21, 3555–3562 (2020). [PubMed: 32749732]

35. Keller L, Werner S & Pantel K Biology and clinical relevance of EpCAM. Cell Stress 3, 165–180 (2019). [PubMed: 31225512]
36. Macdonald J et al. EpCAM Immunotherapy versus Specific Targeted Delivery of Drugs. Cancers 10, 19 (2018). [PubMed: 29329202]
37. Shafraz O, Xie B, Yamada S & Sivasankar S Mapping transmembrane binding partners for E-cadherin ectodomains. Proc. Natl. Acad. Sci. U.S.A 117, 31157–31165 (2020). [PubMed: 33229577]
38. Szklarczyk D et al. The STRING database in 2021: customizable protein–protein networks, and functional characterization of user-uploaded gene/measurement sets. Nucleic Acids Res. 49, D605–D612 (2021). [PubMed: 33237311]
39. Pan M et al. Interactome analysis reveals endocytosis and membrane recycling of EpCAM during differentiation of embryonic stem cells and carcinoma cells. iScience 24, (2021).
40. Huttlin EL et al. Architecture of the human interactome defines protein communities and disease networks. Nature 545, 505–509 (2017). [PubMed: 28514442]
41. Chatr-aryamontri A et al. The BioGRID interaction database: 2017 update. Nucleic Acids Res. 45, D369–D379 (2017). [PubMed: 27980099]
42. Bechtel TJ, Reyes-Robles T, Fadeyi OO & Oslund RC Strategies for monitoring cell–cell interactions. Nat. Chem. Biol 17, 641–652 (2021). [PubMed: 34035514]
43. Reiser A, Willets FW, Terry GC, Williams V & Marley R Photolysis of aromatic azides. Part 4.—Lifetimes of aromatic nitrenes and absolute rates of some of their reactions. Trans. Faraday Soc 64, 3265–3275 (1968).
44. Towns J et al. XSEDE: Accelerating Scientific Discovery. Computing in Science Engineering 16, 62–74 (2014).
45. Bausch-Fluck D et al. The in silico human surfaceome. Proc. Natl. Acad. Sci. U.S.A 115, E10988–E10997 (2018). [PubMed: 30373828]

References (for Methods)

1. Carlson B, Phelan GD, Benedict JB, Kaminsky W & Dalton L Crystal structures and luminescence properties of osmium complexes of cis-1,2-vinylenebis(diphenylarsine) and pyridyl ligands: Possible evidence for metal d, ligand d backbonding. Inorg. Chim. Acta 359, 1093–1102 (2006).

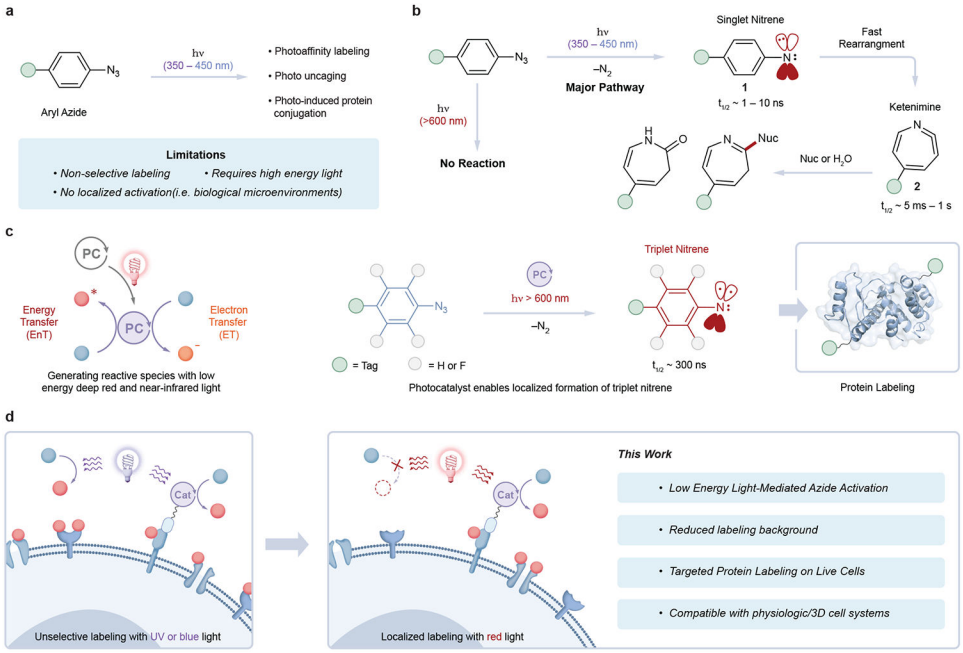

Fig. 1. Selective and targeted uses of aryl azides in chemical biology require low-energy light.

a. Contemporary methods for aryl azide photolysis in chemical biology use high energy light. **b.** Direct azide photolysis proceeds through a singlet nitrene intermediate. **c.** Leveraging electron- or energy transfer mechanisms associated with deep red and near-infrared photoredox catalysis for azide activation. **d.** Targeted aryl azide activation with red light for labeling in biological environments.

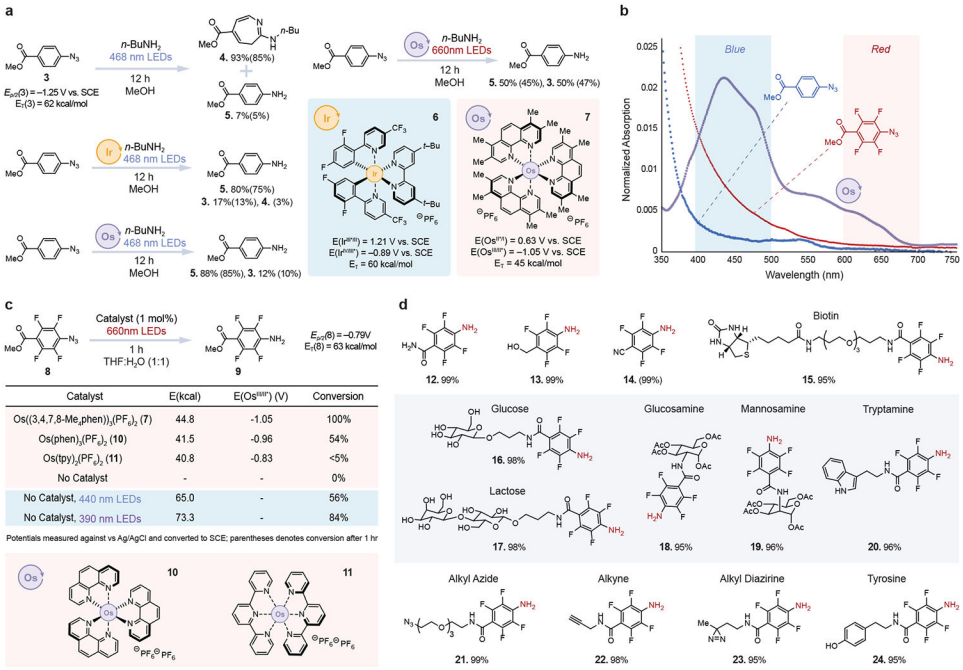

Fig. 2. Deep red photoredox catalysis overcomes fundamental photolytic limitations of aryl azides.

a. Mechanistic investigations into the photolysis and catalytic activation of azides show that the background reactivity is present when using blue light, with isolated yields in parentheses. **b.** Overlaid absorption spectra of unsubstituted azide **3**, perfluorinated azide **8**, and osmium photocatalyst **7**. **c.** Azide-to-aniline reduction studies suggest an electron transfer pathway is operative. **d.** Broad substrate compatibility is observed for azide-to-aniline reduction (See the supplemental information for experimental conditions, ^{19}F NMR yields in parentheses).

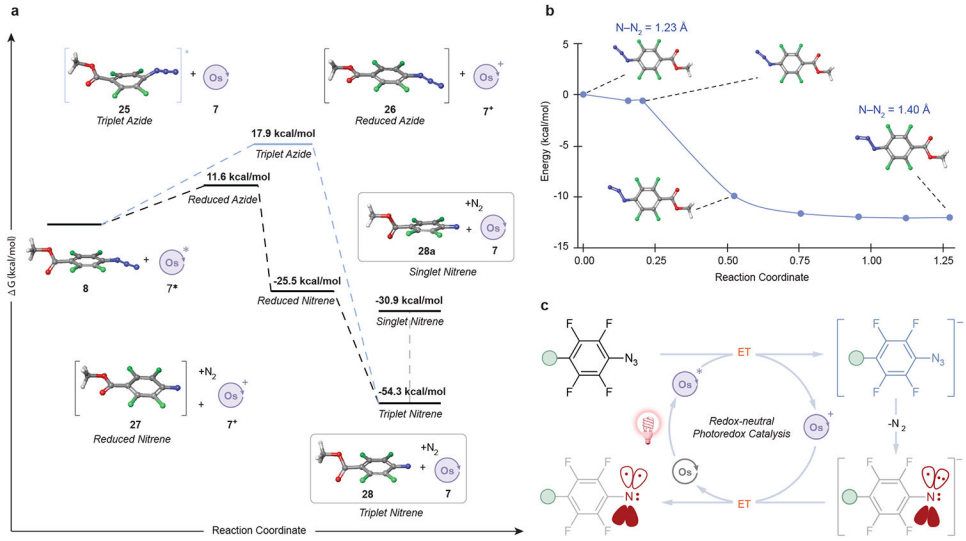

Fig. 3. Computational analysis reveals a redox-neutral, electron-transfer pathway for triplet nitrene formation.

a. A comparison of density functional theory calculated azide-to-triplet nitrene pathways via electron transfer or triplet Dexter energy transfer. B3LYP-D3/CPCM(water)/aug-cc-pVTZ level of theory. **b.** Computational models show that the electron transfer to the azide results in a "barrierless" dissociation of N_2 from the reduced azide. B3LYP/ma-def2-SVP level of theory. **c.** A putative mechanism for accessing triplet nitrenes via a redox-neutral photoredox cycle.

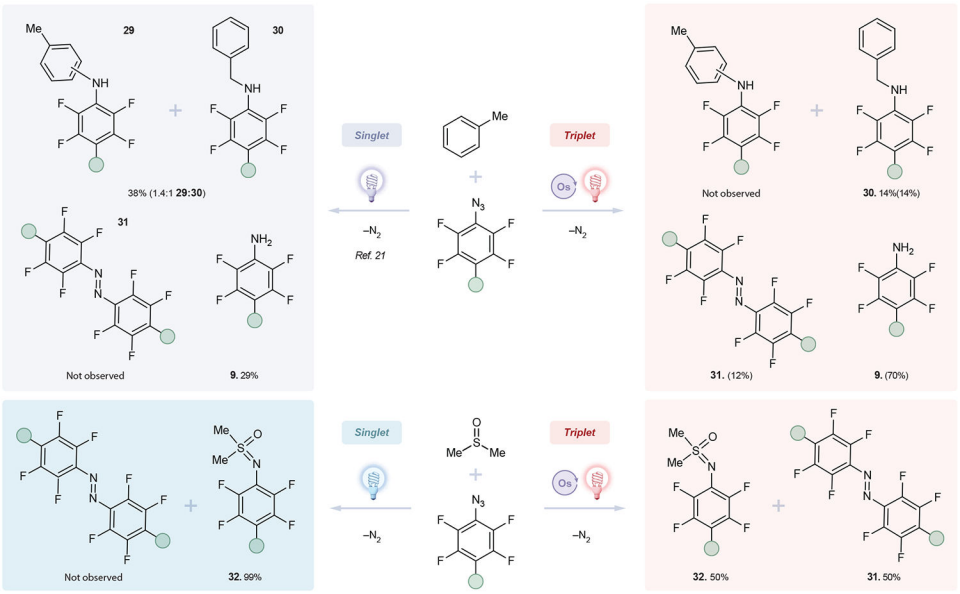

Fig. 4. Mechanistic differences exist between singlet and triplet perfluoroaryl nitrenes.

Distinct reaction pathways are observed for the singlet and triplet nitrenes generated from perfluoroaryl azides, as shown by the products of toluene C–H amination (top) and dimethyl sulfoxide imidation (bottom) (See the supplemental information for experimental conditions, ^{19}F NMR yields are listed in parentheses).

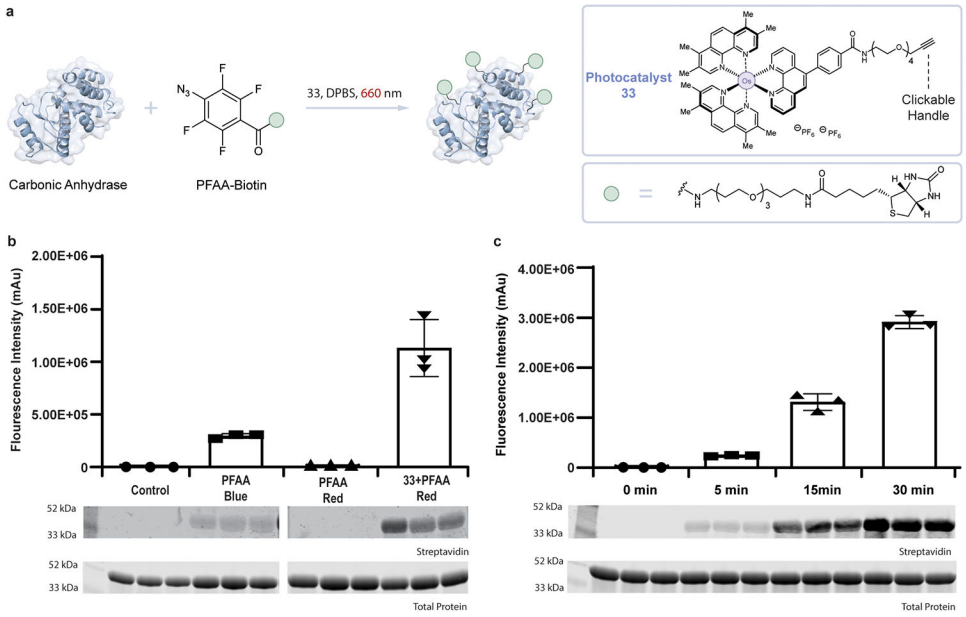

Fig. 5. Deep red light-mediated protein labeling.

a. Schematic depicting labeling of carbonic anhydrase in the presence of osmium-alkyne photocatalyst, PFAA-biotin, and red light. **b.** Western blot image of carbonic anhydrase labeled with PFAA-biotin under different irradiation conditions over 15 min. Selective PFAA activation is only achievable when using a combination of red light and photocatalyst **33**, as background protein biotinylation is observed when using blue light alone. Bar plots of replicate analysis of protein biotinylation measured by western blot. Error bars represent standard deviation of n = 3 experiments. **c.** Time course of protein biotinylation. Western blot analysis shows increased protein labeling over a 30-minute time course. Bar plots of replicate analysis of protein biotinylation measured by western blot. Error bars represent standard deviation of n = 3 experiments.

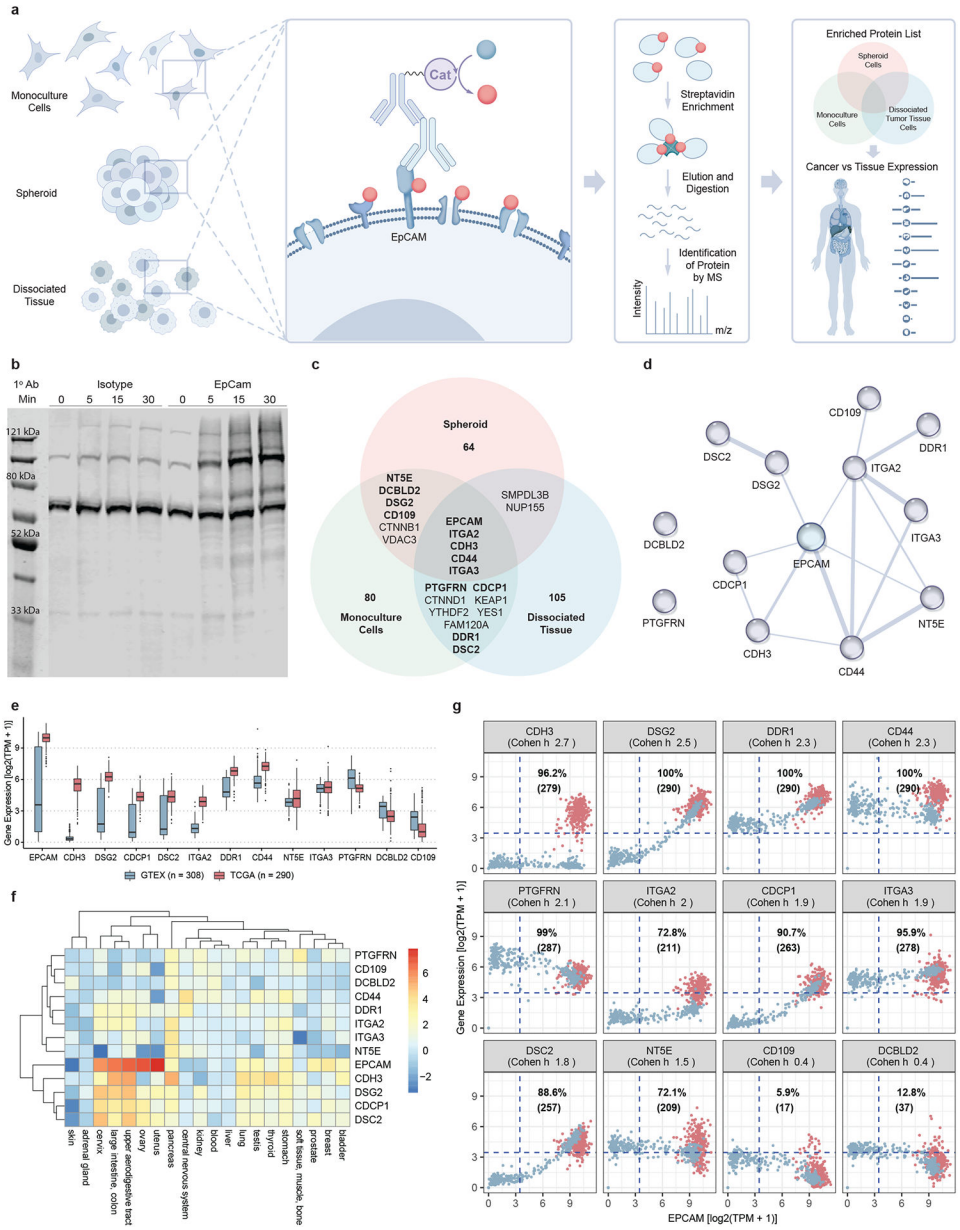

Fig. 6. Deep red light-mediated photocatalytic labeling of cellular environments.

a. Schematic depicting antibody-mediated proximity labeling of EpCAM on the cell surface of different HCT116 cell systems using the osmium photocatalyst system followed by mass spectrometry-based proteomic analysis to identify protein microenvironments for downstream bioinformatic analysis. **b.** Western blot analysis of EpCAM targeted labeling on the surface of HCT116 cells with an α-EpCAM or isotype primary antibody and a secondary antibody photocatalyst conjugate. Increased protein biotinylation is detected with increased DR-light exposure in the presence of the α-EpCAM antibody. Data are representative of n = 2 independent experiments with similar results. **c.** Venn diagram analysis comparing statistically enriched surface proteins identified by proximity labeling in the three different cell systems (total number of enriched proteins in each system is

indicated in the circle). Proteins with known surface expression[45] are highlighted in bold. **d.** STRING protein interaction network analysis of significantly enriched membrane proteins from EpCAM-targeted labeling in different HCT116 cell systems. Line thickness between nodes correlates with experimental evidence of interactions from the STRING database. **e.** Colon Adenocarcinoma primary tumor samples (TCGA, n = 290) vs Sigmoid / Traverse Colon normal tissue samples (GTEx, n = 308) log-fold change of the genes enriched in two or more cell systems highlighted in panel C. Boxplot bounds represent the 25th (Q1) and 75th (Q3) percentile of expression values, with the center indicating median expression. Boxplot length (IQR) equals Q3-Q1. Boxplot whiskers indicate minimum and maximum value with outliers shown as points, and defined as values lower than Q1 - 1.5* IQR and greater than Q3 + 1.5* IQR **f.** Heatmap showing $\log_2$ fold-change between tumor vs normal gene expression across the indicated tumor types. **g.** Scatterplots showing co-expression between EpCAM and the indicated gene in primary tumor colon adenocarcinoma samples from TCGA (red, n = 290) and healthy colon and large intestine samples from GTEX (blue, n = 308). Co-expression is denoted as % tumor samples that expressed both genes at TPM > 10, indicating medium/high expression level (blue, dashed line). The effect size of tumor versus normal co-expression difference is provided as Cohen h for each gene pair.